Shape-induced translational mode transition and self-entrapment of self-propelled metallodielectric rods

Iwashita, Yasutaka
Department of Physics, Kyoto Sangyo University

Kimura, Yasuyuki
Department of Physics, Kyushu University

出版情報：Physical Review E. 113 (5), pp.L053404-, 2026-05-19. American Physical Society (APS)
バージョン：

Supplemental Material for "Shape-Induced Translational Mode Transition and Self-Entrapment of Self-Propelled Metallodielectric Rods"

Yasutaka Iwashita[1] and Yasuyuki Kimura[2]

[1]Department of Physics, Kyoto Sangyo University, 603-8555 Kyoto, Japan.

[2]Department of Physics, Kyushu University, 819-0395 Fukuoka, Japan.

*Correspondence to: iwashita@cc.kyoto-su.ac.jp

S1 Methods

A. Sample preparation

Rectangular rods were produced from the epoxy-based negative photoresist SU-8 2002 (Kayaku Advanced Materials) on glass substrates using standard photolithography (ES20, Nanometric Technology Inc.) [18, 19]. A 25 nm-thick chromium (Cr) layer was thermally deposited onto one width-length face of each rod to create Janus structures (Fig. 1a). The Janus rods were released from the substrate by sonication in Remover PG (Kayaku Advanced Materials) (Fig. 1b). Notably, longer rods exhibited slight bending toward the Cr-coated side (Figs. 1c, d).

The collected rods were rinsed several times with isopropanol, and both the rods and indium tin oxide (ITO)-coated glass plates (1005, Geomatec, 5 Ω/sq) were soaked in a 5.0 wt% aqueous solution of Pluronic F-127 (Sigma-Aldrich Merck) to improve dispersion stability [5,7]. The pretreated rods were dispersed in ultrapure water (18.2 MΩ, Simplicity UV, Merck Millipore), deionized with mixed-bed resin (AG501-X8(D), Bio-Rad), and then mixed with NaCl solution to obtain the final concentration of 0.1 mM. The resulting suspension was confined between the pretreated ITO-coated substrates using a 100 μm-thick silicone rubber spacer, and the chamber was sealed with epoxy glue.

A cylindrical micropillar with 4.0 μm diameter and 14 μm height in Fig. 3c was produced with SU-8 3010 (Kayaku Advanced Materials).

B. Observation and ICEP experiment

After confinement, the two-dimensional dispersion of sedimented rods on the bottom substrate of the sample cell was observed at room temperature using optical microscopes (TE2000-U, Nikon; IX-73, Evident) equipped with cameras (UI-3240LE, IDS Imaging; EO-1312-C, Edmund Optics). Images and videos were analyzed using ImageJ [29]. The speed v of a self-propelled rod is defined as the average of instantaneous speeds measured between consecutive video frames, with frame rates ranging from 2 to 20 fps.

To induce ICEP propulsion, a rectangular AC voltage (frequency $f = 1$ kHz) was applied *via* copper conductive tapes adhered to the ITO-coated substrates. The voltage amplitude V_p ranged from 0 to 10 V. The electric field was applied perpendicular to the confinement planes, *i.e.*, normal to the substrates.

S2 Temporal response and history dependence of translational speed

Figure S1 shows the temporal response of instantaneous translational speed v_i to changes in the applied voltage V_p, where v_i is calculated from two successive video frames. For both horizontal (Fig. S1a) and vertical (Fig. S1c) modes, v_i changed almost instantly ($\lesssim 0.1$ s) upon variation of V_p. Following a change in V_p, a brief overshoot is observed, after which the speed reaches a steady value within a few seconds (see, e.g., the 0 to 4 V change in Fig. S1a and the 2 to 10 V change in Fig. S1c). In the main text, the translational speed v is defined as the steady-state value obtained by averaging the speed over two successive video frames.

For the horizontal mode in Fig. S1a, the speed at $V_\mathrm{p} = 4.0$ V in the 0-2-4-2-0 V sequence reaches the same steady level ($\sim$20 μm/s) as in the 0-4-6-4-0 V sequence. This indicates that the steady-state speed

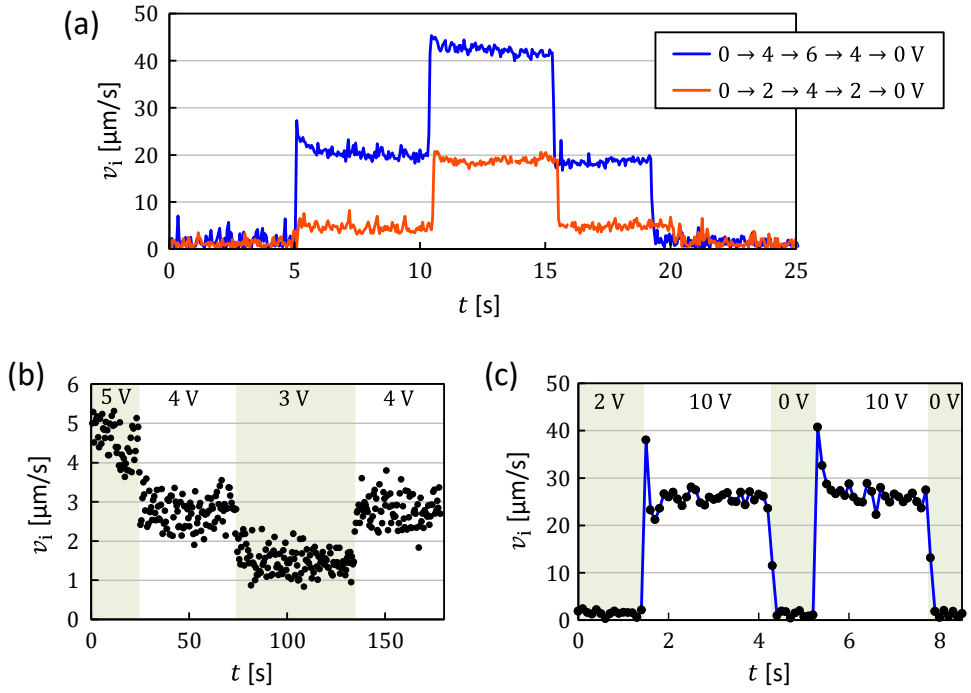

Fig. S1 Instantaneous translational speed v_i of $l = 80$ μm rods as a function of elapsed time t for the sequential changes in V_p shown in the panels. v_i is calculated from two successive video frames. (a) Horizontal mode for two different V_p sequences, obtained from 19.9 fps movies. The same rod was used for both sequences. The upper (blue) plot corresponds to the sequence 0, 4, 6, 4, and 0 V, and the lower (orange) plot corresponds to 0, 2, 4, 2, and 0 V. (b), (c) Vertical mode, obtained from 2.0 fps and 10.0 fps movies in (b) and (c), respectively. The rods observed in (b) and (c) differ from that in (a). In (c), the 0 V interval is short because the rod was laying down; therefore, the second 10V sequence may be influenced by the residual flow fields generated during the first 10V sequence.

is independent of the previous V_p value (0, 2, or 6 V in Fig. S1a). The magnitude of the overshoot at the moment of the V_p jump appears to increase with the corresponding change in steady-state speed.

For the vertical mode, the steady-state speed at $V_\mathrm{p} = 4.0$ V is again independent of the V_p history (Fig. S1b). In this case, the overshoot would be small compared with the scatter in the plot. Figure S1c shows an example of a discernible overshoot in the vertical mode following a large voltage jump.

The observed overshoot is probably related to the development of the macroscopic flow field around the rod. The development of the surface slip flow in ICEP is instantaneous ($\lesssim 10^{-3}$ s in this experiment; see Sec. S4). When the electric field is applied, the surrounding liquid responds to the surface slip flow, and the global flow relaxes toward a steady state over a timescale of a few seconds, as observed in Fig. S1. In the steady state, the surrounding liquid flows opposite to the rod motion, thereby reducing the propulsion speed. When V_p is increased abruptly, the counter-flow is initially weaker than in the new steady state, resulting in transiently higher rod speed (positive overshoot). Conversely, when V_p is decreased abruptly, the counter-flow is initially stronger than in the new steady state, leading to a negative overshoot. For example, during the 6 to 4 V change in Fig. S1a, the speed first decreases and then recovers to the same steady level as in the other 4 V cases. This transient memory in the surrounding flow field makes the V_p-increase and V_p-decrease processes asymmetric. Notably, this asymmetry does not affect the results presented in the main text, which focus on steady-state behavior, and is often indistinguishable, as in Fig. S1b.

S3 Additional data on length dependence of translational modes

Figure S2a shows the transition voltages as a function of rod length, indicating that V_p^up, $V_\mathrm{p}^\mathrm{down}$, and their difference $V_\mathrm{p}^\mathrm{up} - V_\mathrm{p}^\mathrm{down}$ all increase with l. Notably, V_p^up is plotted as 10 V for $l = 80$ μm, corresponding to the upper voltage limit of our setup. In this case, the vertical mode was observed only when a rod accidentally stood upright due to interactions with other rods or with dust particles. In contrast, for $l = 10$ μm, no measurable difference between the transition voltages was detected under our

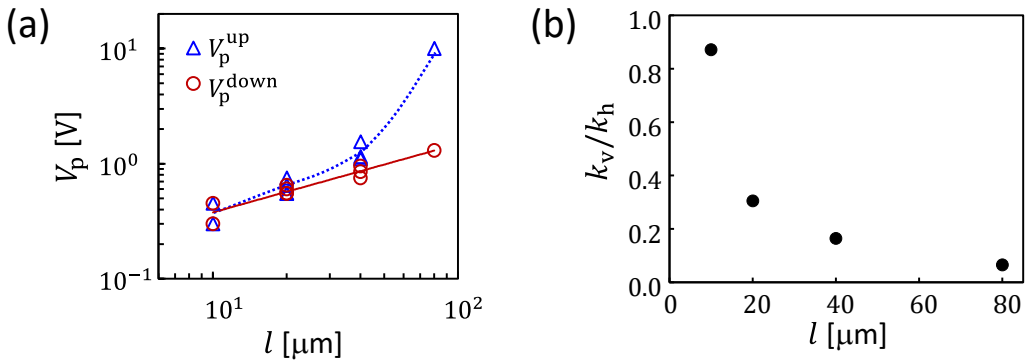

Fig. S2 Length dependence of translational modes. (a) Transition voltages as a function of rod length: V_p^up (triangles) and $V_\mathrm{p}^\mathrm{down}$ (circles). Multiple data points at the same l represent different rods. Data from Fig. 2c are included. The solid line is a fit to $V_\mathrm{p}^\mathrm{down}$, showing $V_\mathrm{p} \propto l^{0.6}$. The dotted line serves as a guide to the eye for V_p^up. (b) Ratio k_v/k_h from Fig. 2d, representing the speed ratio between the horizontal and vertical modes.

experimental conditions.

Figure S2b shows that the relative deceleration upon reorientation into the vertical mode decreases with increasing l.

S4 ICEP speed of a metallodielectric Janus cylinder

As written in the main text, the ICEP speed of an infinitely long metallodielectric Janus cylinder aligned perpendicular to the applied electric field is given by [21,23]

$$v = \frac{4}{3\pi}\frac{\varepsilon a}{\eta(1+\delta)}E^2 ,$$

where $E = V_\mathrm{p}/100$ [V/μm]. The viscosity and permittivity of the medium are taken as $\eta = 0.8902 \times 10^{-3}$ Pa · s and $\varepsilon = 6.938 \times 10^{-10}$ F/m, corresponding to those of pure water since the added salt concentration is low [30]. We assume $\delta = 10$, following the estimation by Gangwal *et al.* [23], and take $a = w/2 = 1$ μm, where aE corresponding to the induced surface potential ζ_i. Using these parameters, we obtain the proportionality constant $k_\mathrm{h} = v/{V_p}^2 = 3.0$ μm/V² · s.

S5 l-dependence of k_v

The diffusion constant used for calculating the RC charging time is $D = 1.683 \times 10^{-9}$ m²/s, corresponding to the average of the diffusion constants of $\mathrm{Na^+}$ and $\mathrm{Cl^-}$ (1.334×10^{-9} m²/s and 2.032×10^{-9} m²/s, respectively), extrapolated to 0 M [30]. The deviation of these values at 0.1 mM is expected to be negligible. The Debye screening length is taken as $\lambda = 30.4$ nm for a 0.1 mM NaCl aqueous solution [31]. The inverse of the RC charging time, ${\tau_\mathrm{p}}^{-1}$, where $\tau_\mathrm{p} = \lambda x/2D$, is plotted in Fig. S3 for $x \leq 100$ μm.

The comparison between the two scaling relations, $k_\mathrm{v} \propto \frac{1}{1+\omega^2\tau_\mathrm{p}^2}$ and $k_\mathrm{v} \propto \frac{l}{1+\omega^2\tau_\mathrm{p}^2}$, is shown in Fig. S4. For the latter, the numerator term l causes an initial increase in k_v with rod length, which is opposite to the experimental trend.

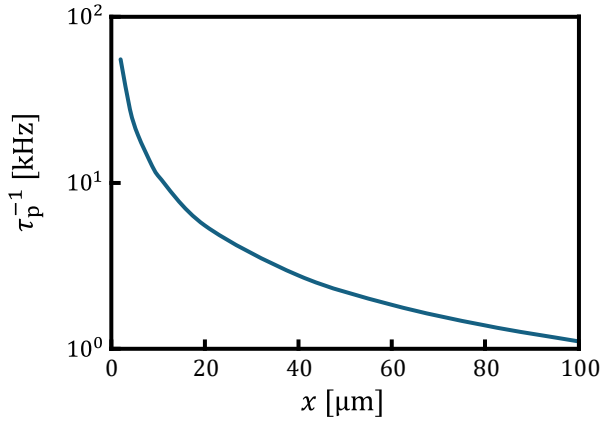

Fig. S3 Plot of τ_p^{-1} as a function of x.

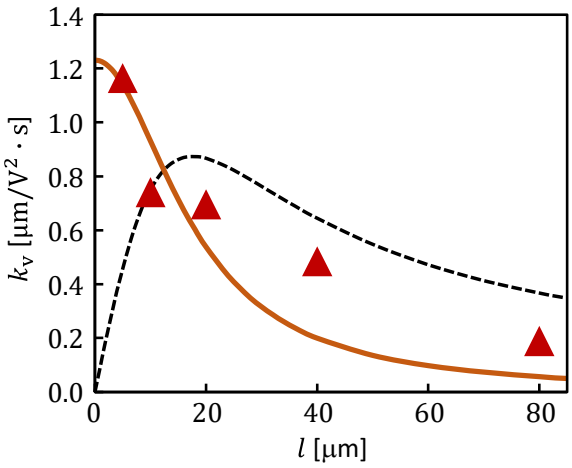

Fig. S4 Comparison between $k_v \propto \frac{1}{1+\omega^2\tau_p^2}$ (solid line) and $k_v \propto \frac{l}{1+\omega^2\tau_p^2}$ (dashed line), fitted to the experimental data.

S6 Additional data for self-entrapment and oscillation

Figure S5 presents additional data related to Figs. 3 and 4. Figure S5a shows a representative example of the self-entrapment and oscillation process of an $l = 80\mu m$ rod.

The $d - \theta$ plots in Fig. S5b indicate that the oscillatory dynamics form a limit cycle, with the rod's motion corresponding to an attractor. At constant V_p, the oscillation traces a closed orbit with fluctuations (blue and yellow lines). When V_p is changed, the trajectory transitions to a new orbit (solid black line). In contrast, a stable orbit (attractor) is not identified at low voltage as shown in Fig. S5c. This suggests that thermal and/or athermal perturbations are large compared to the stability of the limit-cycle motion at small V_p. Nevertheless, the averaged oscillation amplitude and period remain measurable and exhibit systematic trends, as shown in Fig.4b. No additional stable kinetic modes (attractors) were observed in our experiment.

The ratio A_θ/p_θ is plotted in Fig. S5b, which qualitatively represents the speed of the oscillating rod. The trend suggests a possible linear dependence on V_p^2 above a threshold, not contradictory to the translational speed scaling in Figs. 2b and c.

Next, we present additional data to demonstrate the stability and reproducibility of the oscillatory motion. Figure S6a shows a representative 200 s time series of the oscillatory motion. The oscillation is not perfectly stable but exhibits temporal fluctuations in amplitude and period on a timescale of ~10 s. Table S1 compares the amplitudes and periods measured at the same V_p under four different histories: (#1) preceding V_p smaller than the measurement value, (#2) preceding V_p larger than the measurement value, (#3) preceding $V_p = 0$, i.e., the data after turning on the electric field, and (#4) repetition of the process in #3. Despite the different histories, the four measurements yield similar amplitudes and periods considering the intrinsic fluctuations of the motion (see Fig. S6a). Thus, under our experimental conditions, the oscillatory motion represents a stable and reproducible kinetic mode. However, we do not exclude the possibility that other kinetic modes (e.g., steady rotation around an obstacle) may emerge

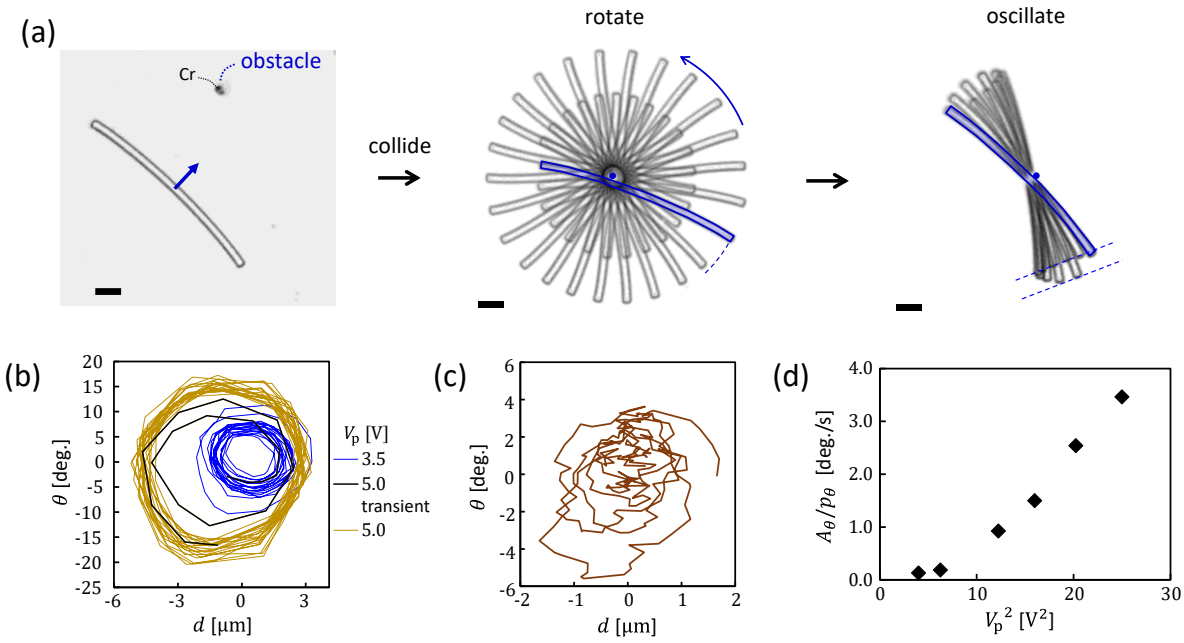

Fig. S5 Additional data on self-entrapment and self-excited oscillation. (a) Overlaid microscopy images (4s intervals) generated using ImageJ's "Z Project" function. An $l = 80$ μm rod collides with a vertically adhered rod (left), rotates (center), and oscillates (right). Applied voltages are $V_\mathrm{p} = 1.3$ V (left/center) and 3.2 V (right). Scale bars: 10 μm. (b) $d - \theta$ plot for the V_p-change from 3.5 to 5.0 V in Fig. 4a. Thin blue line, thick black line, and thin yellow line correspond to the oscillation at 3.5 V, during the first 10 s at 5.0V, and after 10 s at 5.0 V, respectively. The shift in the center of the circular orbits at 3.5 and 5.0 V reflects the slight asymmetry in the oscillation, as shown in Fig. 3e. (c) $d - \theta$ plot corresponding to the oscillation at $V_\mathrm{p} = 2.0$ V in Fig. 4a. (d) Ratio A_θ/p_θ, derived from Fig. 4b.

under substantially different experimental conditions, such as specific initial rod positions or different V_p histories. It should also be noted that the obstacle size in Fig. S6 and Table S1 differs from that in Fig. 4; therefore, the amplitudes and periods cannot be directly compared with those in Fig. 4b.

Figure S6b shows that the rod motion ceases rapidly when the voltage is turned off, consistent with the translational behavior (cf. Fig. S1). When the electric field is reapplied after a pause, the oscillation does not resume from its previous phase, in contrast to, for example, stable active pair clusters exhibiting helical motion in bulk liquid [9]. This behavior is consistent with the overshoot observed in translation (Fig. S1): the surrounding flow field differs between the initial transient and the steady state, so the hydrodynamic conditions at restart are not identical to those at the moment when the previous motion stopped. If the pause were sufficiently short that the surrounding flow field had not yet relaxed, the oscillation might continue from the previous phase.

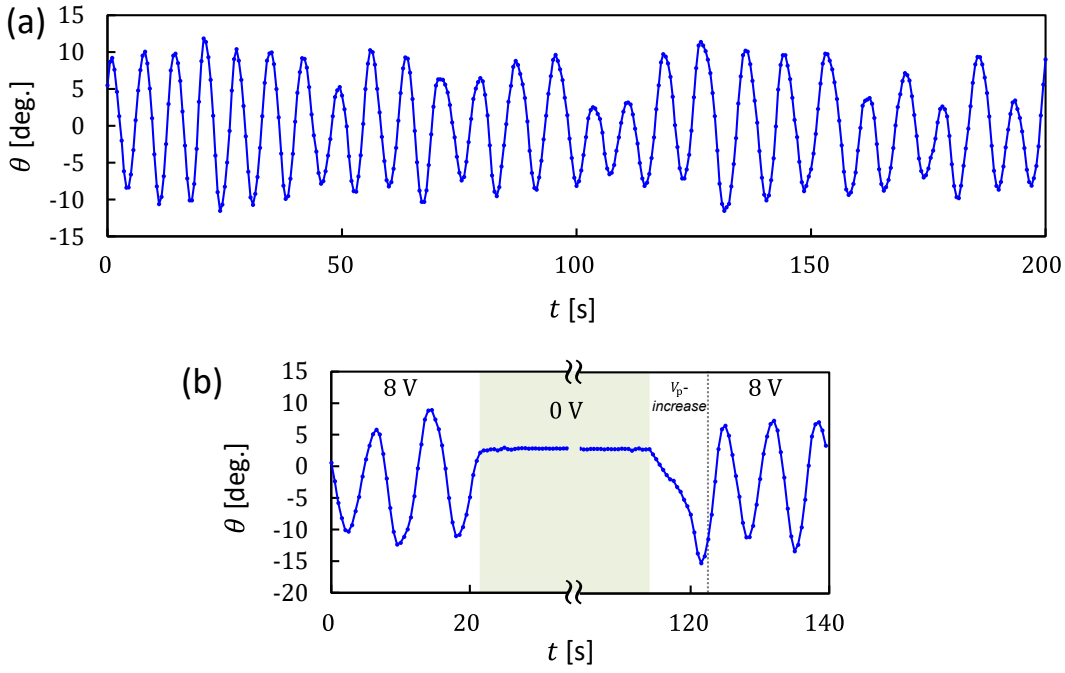

Fig. S6 Temporal evolution of the rod angle θ for an $l = 80$ μm rod around a cylindrical SU-8 micropillar (8.0 μm diameter, 11 μm height), obtained from a 2 fps movie. (a) θ during a selected 200 s at $V_\mathrm{p} = 8.0$ V. (b) θ for the sequential changes in V_p shown in the panel. From 0 V to 8 V, V_p was gradually increased over 9 s.

Table S1 Angular oscillation amplitude A_θ and oscillation period p_θ of the rod in Fig. S6 at $V_\mathrm{p} = 8.0$ V for four measurements (#1–#4). Figure S6a corresponds to measurement #3, and Fig. S6b corresponds to the process from #2 to #3. The duration of the preceding $V_\mathrm{p}$in each case exceeds 1 min. For #3 and #4, V_p was gradually increased over 9 s, whereas for #1 and #2, V_p was changed instantaneously. The analyzed oscillation duration in each case is ≳300 s.

#	1	2	3	4
preceding V_p (V)	7.0	9.0	0.0	0.0
A_θ (deg.)	9.5	8.3	8.3	7.8
p_θ (s)	9.1	7.8	7.7	8.1